SSC22-VII-02

Empirical Methods for Reaction Wheel Micro-Vibration Verification in a Production Environment

Sobia Nadeem
McMaster University
nadees13@mcmaster.ca

Faculty Advisor: Brent Brakeboer
Sinclair Interplanetary by Rocket Lab

ABSTRACT

There is great interest in high precision attitude control of satellites, in particular for missions that operate payloads with stringent pointing requirements. Reaction Wheels (RW) are an integral part of a satellite's Attitude Determination and Control System (ADCS). However, a drawback of using RWs is that due to imperfections such as rotor imbalance and bearing defects, RWs are a source of micro-vibration. These phenomena can lead to internal disturbances which in turn may lead to degraded mission performance.

Quantifying the micro-vibration generated by RWs is a critical and time intensive process. A two-step process to verify and characterize RW micro-vibration performance will be presented in this paper. The verification is performed by conducting a short-form test in a single axis using a Laser Doppler Vibrometer (LDV). The characterization is performed by conducting a long-form test in all axes using a Multicomponent Force Dynamometer. Both tests allow for the determination of a RW's imbalance and noise profile which can be evaluated against a pass/ fail criteria.

A challenge associated with scaling production is verifying wheel micro-vibration performance in an efficient manner, while maintaining a high degree of product assurance. Quality control limits and correlation analyses were conducted to aid in developing a more efficient process for RW verification and characterization. A framework for the refined two-step process will be presented alongside a case study to identify acceptable micro-vibration performance, using Sinclair Interplanetary's RW-0.06 product. The methods presented here can be used within the small satellite community to better understand and predict the micro-vibration performance of reaction wheels.

INTRODUCTION

Reaction wheels (RW) provide precision pointing capability and are vital to a satellite's Attitude Determination and Control System (ADCS). They operate on the principle of conservation of angular momentum, allowing for a spacecraft to perform attitude maneuvers on-orbit without expending fuel. An electrical motor is used to rotate the wheel, which causes the spacecraft to counteract this movement by rotating in the opposite direction. A RW is only able to produce a torque about a single axis of rotation. For full 3- axis control, a spacecraft requires at least three RWs along mutually perpendicular axes.

Due to imperfections, RWs are also a source of micro-vibration that can degrade the precision pointing control and performance of other subsystems. Micro-vibrations can be caused by rotor imbalances and bearing imperfections and can be amplified by the RW's structural frequencies. With the growing interest in utilizing small satellite missions for payloads with stringent pointing requirements, such as scientific imaging payloads, there is a greater need to characterize and verify the micro-vibration performance of a RW [1].

This paper studies two methodologies for determining a RW's micro-vibration performance: 1) characterization using a Multicomponent Force Dynamometer and 2) verification using a Laser Doppler Vibrometer (LDV). The characterization process determines both the static and dynamic imbalance present in the RW, and the verification process determines just the static imbalance. Both tests obtain the noise profile in frequency ranges of interest. NASA Jet Propulsion Laboratory (JPL) has utilized a force dynamometer for reaction wheel characterization, similar to the method

presented here [2]. However, to the authors knowledge, the LDV verification framework presented in this paper has not been used for RW applications. The primary RW model used here, is the RW-0.06 product manufactured by Sinclair Interplanetary.

REACTION WHEEL IMBALANCE

The primary RW micro-vibration source that will be explored in this paper will be the rotor imbalance, specifically the static and dynamic imbalances.

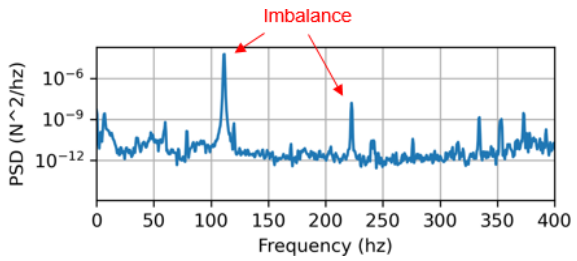

Figure 1: A PSD vs. Frequency Plot that Illustrates a Wheels Imbalance and Resonances

Static imbalance is defined as an uneven distribution of mass in parallel and offset from the axis of rotation, (seen on the left in Figure 2). This imbalance can cause the rotor to move vertically up and down [3]. The static imbalance can be calculated using the following equation:

$$F_c = mr\,\omega^2 \tag{1}$$

The static imbalance is the product of the imbalance mass (m) and the radial distance (r) of the mass from the axis of rotation and is in unit's *gram-mm*. The centripetal force (F_c) produced by the rotor can be divided by the square of the rotation speed (ω) to obtain the static imbalance.

Dynamic imbalance is defined as an uneven distribution of mass that is not parallel with the axis of rotation (seen on the right in Figure 2). This results in a nonzero angle between the axis of inertia and the axis of rotation. This type of imbalance can cause the rotor to wobble [3]. Similarly, the dynamic imbalance can be calculated using the following equation:

$$M = mrd\,\omega^2 \tag{2}$$

Where M is the transverse moment produced by the rotor. The dynamic imbalance is defined as *mdr*, where d is the distance along the axis of rotation and is in units of *gram-mm*^{2}.

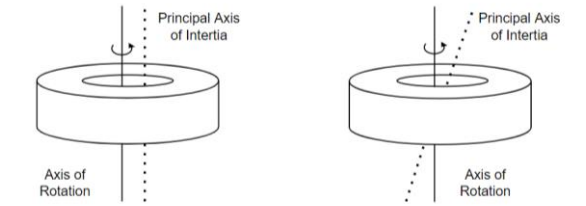

Figure 2: Static Imbalance (left) and Dynamic Imbalance (right)

MULTICOMPONENT FORCE DYNAMOMETER

The principal component of the multicomponent force dynamometer are the piezoelectric force sensors that are placed between the dynamometer plates. Piezoelectric sensors are made up of two crystal disks that have an electrode foil in between them. When a force (F) is applied, an electrical charge (Q) is produced which can be calculated using the following equation:

$$Q = q_{xy}F \tag{3}$$

Where q_{xy} is the piezoelectric constant. The charge produced can then be measured with a charge amplifier. The charge is proportional to the force applied. These sensors offer high stiffness, resulting in a high resonance frequency that is desirable for dynamic applications [4].

Data Acquisition System

Kistler's multicomponent piezoelectric force dynamometer was used to characterize the Exported Force and Torque (EFT) generated by the RWs. The device has four 3-component force sensors that are processed using a multichannel charge amplifier. The charge amplifier allows for characterization of micro-vibration disturbances in three axes of force and torque, using equations 4-9:

$$F_x = F_{x1+2} + F_{x3+4} \tag{4}$$

$$F_y = F_{y1+4} + F_{y2+3} \tag{5}$$

$$F_z = F_{z1} + F_{z2} + F_{z3} + F_{z4} \tag{6}$$

$$M_x = b * (F_{z1} + F_{z2} - F_{z3} - F_{z4}) \tag{7}$$

$$M_y = a * (-F_{z1} + F_{z2} + F_{z3} - F_{z4}) \tag{8}$$

$$M_z = b * (-F_{x1+2} + F_{x3+4}) + a * (F_{y1+4} - F_{y2+3}) \quad (9)$$

In equation 7-9, a and b are vertical and horizontal separations from the center of the force sensors to the centerline of the dynamometer [5]. The data acquisition is conducted using the force dynamometer compatible software, the Multi Device Client.

The force dynamometer was centered on top of a granite table with pneumatic isolation at each corner, to reduce seismic vibrations. To verify the natural frequency response of the dynamometer, an impact hammer was used to determine the system's Frequency Response Function (FRF). The transfer function was determined using the hammer as the input and the response of the dynamometer as the output. The first resonance frequency in the FRF graph (seen in Figure 3), is at approximately 1250 Hz. To ensure there is no amplification in the measurement frequency range, the frequency range of interest was further limited to <400 Hz.

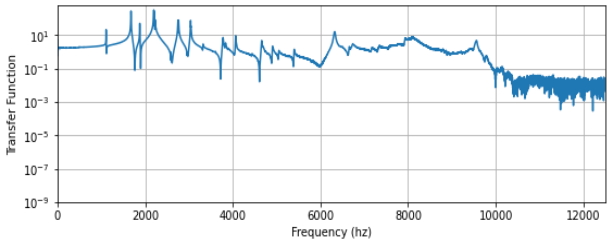

Figure 3: Fy FRF Determined by the Impact Hammer

Test Profile

The force dynamometer characterization was performed on all RW types greater than RW-0.06 manufactured by Sinclair Interplanetary. This section will illustrate the test profile and results of this characterization for the RW-0.06. Due to its small size, the RW is first mounted to a custom interface plate that is then secured to the center of the dynamometer (as seen in Figures 4 and 5).

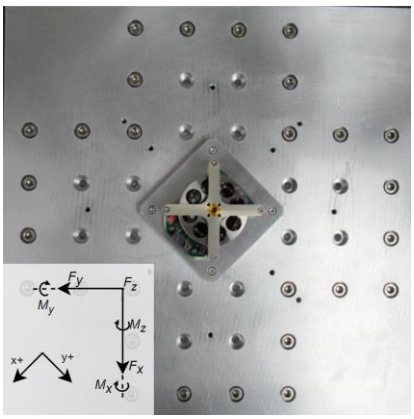

Figure 4: Top View of the RW-0.06 Product

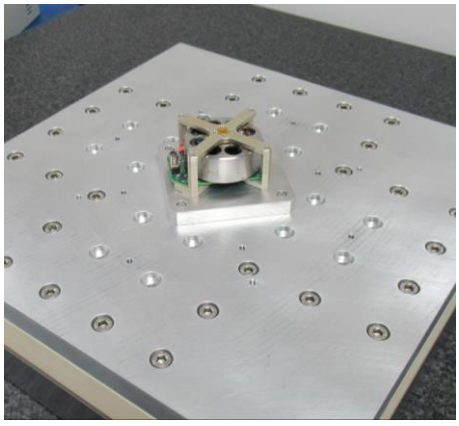

Figure 5: View of the RW-0.06 Product Attached to the Dynamometer by an Interface Plate

The standard test profile for the characterization test was refined to two key phases: Phase 1 steady state measurement and Phase 2 sweep measurement. The first phase of the test began at the RW's maximum speed, where steady state conditions were measured for approximately 30 seconds. In the second phase, the wheel was commanded to brake by -0.5 rad/s from maximum speed, which began the sweep measurement. Once the wheel reached 0 rad/s, phase 2 was complete and the data was exported. The Phase 1 steady state data was processed using coherent integration to determine the RW's static and dynamic imbalance. The Phase 2 sweep data was used to generate the waterfall plots, which are detailed in the following section. The duration of this test was approximately 20-40 minutes depending on the RW product used.

Data Processing and Analysis

The data was initially pre-processed using a zero-phase Butterworth filter with a cutoff of 1000Hz. It was then subsampled and compressed to reduce storage requirements without compromising the data integrity.

To process the Phase 1 steady state data, the data was isolated from Phase 2 in order to calculate the static and dynamic imbalance by coherent integration, using equations 10 and 11 respectively:

$$\boldsymbol{Im_x} = \frac{\boldsymbol{2(\theta \cdot F_x)}}{\boldsymbol{n\omega^2}}, Im_y = \frac{2(\theta \cdot F_y)}{n\omega^2}, Im = \sqrt{Im_x^2 + Im_y^2} \quad (10)$$

$$\boldsymbol{Im_x} = \frac{\boldsymbol{2(\theta \cdot M_x)}}{\boldsymbol{n\omega^2}}, Im_y = \frac{2(\theta \cdot M_y)}{n\omega^2}, Im = \sqrt{Im_x^2 + Im_y^2} \quad (11)$$

Where $\emptyset$ = phase (radians), F = measured force in the x-direction, M = measured moment in the x-direction, Im = imbalance, n = number of samples, and ω = wheel speed (rad/s).

Coherent integration was used as it can significantly improve the signal-to-noise ratio (SNR). Phase knowledge was required to calculate the imbalances with this method, which can be found using a tachometer. A simulated tachometer was used in this case, as it is the simplest implementation. It should be noted that a simulated tachometer does not provide exact phase knowledge, however this is not a concern for the purpose of the characterization described here. Therefore, refining the setup to include an optical or electrical tachometer at the production level of testing was not justified.

To process the phase 2 data, the data was segmented twice, creating two components of the dataset. The first component was used to check that the speed per segment was approximately constant. The second component allowed for averaging of the measurement in the frequency domain. Each segment was multiplied with a Hann window followed by a real-to-complex Fast Fourier Transform (FFT). The magnitude was then squared and averaged. The output was a Linear Spectrum (LS) for each segment in the first component, which can then be converted to Power Spectral Density (PSD). To convert from the LS to PSD, the LS is squared and then divided by the Effective Noise Bandwidth (ENBW). The processed data was visualized using a waterfall plot which has axes LS vs. Speed vs. Frequency or PSD vs. Speed vs. Frequency (as seen in Figure 6).

The test profile and processing allowed for a total characterization of the RW EFT across its operating speed range. The outputs of this processing are the imbalances and waterfall plots for each axis of force and moment. The imbalances can be used to determine if the wheel meets the standard defined by the quality control limits. The PSD information can be used in a spacecraft micro-vibration profile to understand potential coupling modes or excitation degradation. The waterfall plots illustrate the RW imbalance, and the environmental vibrations present during the test.

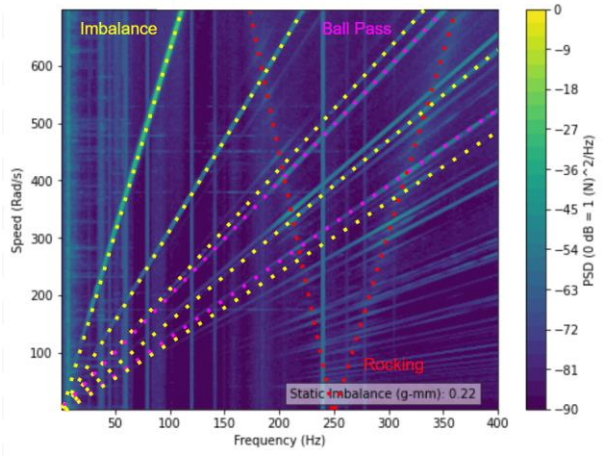

Figure 6: PSD vs. Speed vs. Frequency graph in the Fx direction

The above waterfall plot has been annotated to emphasize the main modes determined from this characterization. The fundamental frequency and harmonics of the imbalance and ball pass vibrations from the bearings are highlighted, along with a rocking mode that originates at 250 Hz. Environmental noise in the form of vertical lines can be viewed at various frequencies, due to the broad range of frequencies plotted.

Validation Testing

To validate the force dynamometer for RW characterization, two imbalance tests were conducted using a poorly balanced RW-1.0 manufactured by Sinclair Interplanetary. The purpose of the first test was to validate the force dynamometer measurement with the addition of a known mass. The second test was to verify the use of the force dynamometer to correct a measured imbalance.

The standard test profile for the following validation tests was a 60 second steady state measurement at 300 rad/s. An optical tachometer was used during the validation tests to ensure accurate phase knowledge.

To validate the measurement, a weight of 0.05g and 0.13g was placed on the rotor at 90° and 180°. The results of the tests can be seen in Table 1.

Table 1: Results from the Validation Measurement tests, using a RW-1.0 Product

		Measured imbalance (g-mm)			
Angle (deg)	**Weight (g)**	**x**	**y**	**Magnitude of imbalance**	**Estimated Real Angle**
90	0.05	-0.35	-3.19	3.21	83.82
180	0.05	-2.78	-0.26	2.79	174.74
90	0.13	-0.23	-9.94	9.95	91.3
180	0.13	-3.89	-0.36	3.92	185.2

The estimated real angle found, using the measured x and y components of imbalance, indicate that the calculated location of the weight on the rotor is accurate to where it was placed. This validates that the assumed reference frames and orientation of the RW on the dynamometer plate are accurate.

The verification test was then conducted using a similar process. The static imbalance occurs in one axial plane and can be corrected for by adding a weight that is of equal mass to the imbalance at a 180° offset from the measured imbalance (seen in Figure 7).

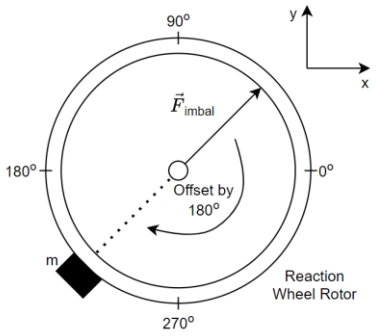

Figure 7: Schematic for correcting the Static Imbalance

First, the RW underwent a control test, to determine the imbalance. The angle of imbalance of the control test was found to be at ~64.8° on the rotor. In theory the imbalance would be corrected at an offset of 180° from the measured imbalance angle, meaning the imbalance should be corrected at ~244.8° on the rotor. Weights of varying mass were placed at angles approximately around 244.8° on the rotor, to correct the imbalance.

The test results can be seen in Table 2. It was found that the imbalance was nearly negligible at ~218°. There is a degree of uncertainty with regards to the mass's exact placement on the rotor, thus the estimated real angle was calculated to verify the results. This means that the imbalance was negligible using a mass of 0.011g at 226°.

Table 2: Results from the Imbalance Correction Verification Tests, using a RW-1.0 Product

		Measured imbalance (g-mm)			
Angle (deg)	**Weight (g)**	**x**	**y**	**Magnitude of imbalance**	**Estimated Real Angle**
-	-	0.35	-0.73	0.81	64.8
250	0.015	0.47	0.45	0.66	315.9
235	0.012	0.21	0.13	0.25	328.6
223	0.012	0.007	0.13	0.13	273
218	0.011	-0.06	0.06	0.08	226

The results of these tests validate the test setup and indicate that the force dynamometer can be used to isolate and correct for a RW's static imbalance.

LASER DOPPLER VIBROMETER

The principle for the Laser Doppler Vibrometer's (LDV) operation is constructive and destructive optical interference, where two coherent light beams with individual light intensities (I_1 and I_2) overlap. The interference term is described as follows:

$$I_{total} = I_1 + I_2 + 2\sqrt{(I_1 I_2 cos[2\pi(r_1 - r_2)/\lambda} \quad (12)$$

The velocity of the object measured using an LDV can be stated as proportional to the modulation frequency of the interferometer pattern. The LDV can detect the object's direction of movement due to an added Bragg cell in the reference beam that shifts the light frequency. This shift is nominally 40 MHz. As the object moves in the direction of the interferometer, the LDV's frequency modulation receives a frequency greater than the shifted light frequency. As it moves towards the object, the frequency received is less than the shifted light frequency [6].

Data Acquisition System

To verify the RW's static imbalance and noise profiles, Polytec's Laser Doppler Vibrometer (LDV) was used for the measurements. The LDV is a non-contact device that determines the vibration velocity and displacement in a single axis. This device is based on the Doppler effect, measuring the Doppler frequency shift of scattered light from a moving component. The Doppler frequency can be calculated as follows:

$$f_D = 2\frac{v}{\lambda} \quad (13)$$

Where v = velocity of component and λ = wavelength of emitted light [6].

The vibrometer setup was located inside of a flow hood for cleanliness. The RW was placed inside of an unfixed 3D printed cradle. The cradle was positioned on top of a lifted metal plate that was in line with the laser emitted from the LDV (as seen in Figures 8 and 9). The metal plate has screwheads that the cradle was firmly pushed against, to ensure that the position of the RW was consistent across tests with different RWs of the same size. For optimal use, the laser was placed approximately 5.5cm from the standoff where the RW was mounted.

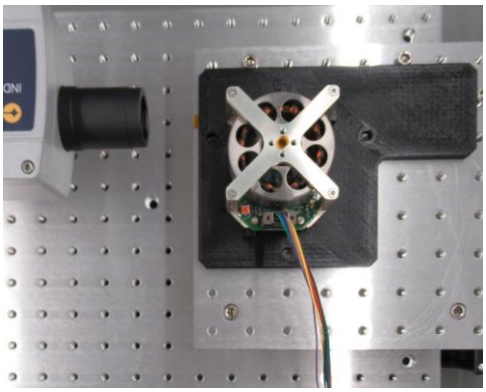

Figure 8: Top View of the RW-0.06 Product

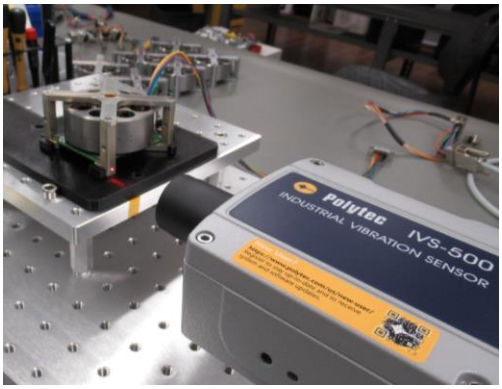

Figure 9: View of the RW-0.06 Product Placed on a Standoff in Line with the Laser Doppler Vibrometer

To reduce the noise in the measurement, viscoelastic dampers were placed underneath each corner of the steel plate on which the LDV was mounted. It was found that the addition of the dampers reduced the noise significantly in the lower frequency range (0-150 Hz) starting at 30Hz and had damping effects up to the middle frequency range (150-2000 Hz) (as seen in Figure 10). At higher frequency ranges (2000-10000 Hz) it was found that the dampers had little to no damping effects.

Figure 10: Low Frequency Range (top) and Medium Frequency Range (bottom). The Blue Line Indicates the System without Viscoelastic Dampers, and the Orange Line Indicates the System with Viscoelastic Dampers

Test Profile

The laser doppler vibrometer RW verification was performed on all RW types manufactured by Sinclair Interplanetary.

The standard test profile for the verification using the LDV was to take a single-shot measurement once the wheel reached 600 rad/s. The LDV measurement was output in the frequency domain with a standard of 12800 FFT Lines, a bandwidth of 10 kHz, and a Hann window applied. The duration of this test was approximately 5-10 seconds, regardless of the RW product used.

Data Processing and Analysis

The data was processed using a custom software package in python. The frequencies were segmented into low (0-150 Hz), medium (150-2000 Hz) and high (2000-10000 Hz) frequency ranges. The data collected from the LDV was represented as a power spectral density with units a^2/HZ. To convert from PSD to LS, the data was multiplied by ENBW and square rooted to obtain the LS acceleration with units RMS.

$$a_{LS} = \sqrt{a_{PSD} \cdot enbw} \tag{14}$$

The static imbalance was determined using the following equation:

$$Im = \frac{m\sqrt{2}a_{LS}}{\omega^2} \quad (15)$$

Knowledge of the mass that is excited during the LDV test was unknown, therefore, to convert the acceleration to a force, the excited mass was assumed to be 1kg.

At 600 rad/s, it was observed that a RW's imbalance presented as a large peak at ~95 Hz, with a smaller resonance peak at ~190 Hz (seen in Figure 11). Other peaks may be observed with a variety of causes such as bearing imperfections.

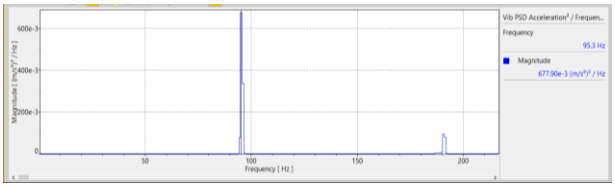

Figure 11: Imbalance peak at 95 Hz and resonant imbalance peak at ~200 Hz, seen in a RW-0.06 product at 600 rad/s

A Hann window and FFT were applied in the measurement software prior to the data output, thus the only processing required was to split and plot the data. The processed data output a PSD vs. Frequency graph, for each of the frequency ranges.

Validation Testing

The LDV is an efficient procedure to verify the RW's static imbalance, due to the short duration of the test and simple setup. This is useful in a production environment as multiple tests can be efficiently performed at different points of acceptance testing, which allows for consistent monitoring of the RW's micro-vibration profile.

Although the LDV was efficient, the test method had a low repeatability rate. This warranted further tuning of the setup to better understand the optimal bandwidth for testing, to increase repeatability between tests.

To tune the LDV, three sets of tests were performed, with an FFT Line frequency bandwidth of 10, 5 and 4 kHz. A sample of 30 measurements were collected at each bandwidth, with the results shown in Table 3. At 4 kHz the standard deviation in the results of 30 measurements was significantly reduced.

Table 3: Standard Deviation and Average of the RW-0.06 Products Static Imbalance Using the Laser Doppler Vibrometer

Frequency Bandwidth (kHz)	Standard Deviation	Average Static Imbalance
10	0.2	8.03
5	0.1	7.09
4	0.09	7.46

It should be noted that there will still be a degree of variability in the results between different RW's, simply due to the RW being unfixed in the test setup. However, to maintain the efficiency of the test, the author did not explore further adjustments to the test setup to reduce all sources of variability.

RESULTS

There is a desire to refine the two-step process presented, to efficiently verify a RW's micro-vibration performance. Currently every RW of type RW-0.06 or larger manufactured by Sinclair Interplanetary, undergoes both the long form characterization test using the force dynamometer and the short form verification test using the LDV. This was done to obtain a large data set to compare the data collected by both methods. To validate a refined two-step process, quality control limits, a correlation analysis, and a case study to illustrate the pass/fail criteria is presented in this section.

Quality Control Limits

To create specifications for an acceptable RW micro-vibration profile, it is necessary to create a set of quality control limits. This can be done either analytically or qualitatively using a large set of data. Both approaches will be used here, to find the quality control limits of the static imbalance and noise profiles using both the force dynamometer and LDV. This analysis will be conducted using a sample of approximately 85 independent measurements of the RW-0.06 product.

The analytical approach utilizes the statistical calculation of 3-sigma, which is commonly used to set upper and lower limits for quality control. These quality control limits are found by calculating three standard deviations from the mean of a series. The resulting value is the upper and lower control limits for a data set. The 3-sigma upper control limits were found for the static imbalance and noise profiles. The lower control limits were not accounted for as it is desirable for the static imbalance and noise profile values to be as low as

possible. This analysis can be plotted using a histogram and normal distribution function to illustrate the quality control limits found analytically (seen in Figures 12 and 13).

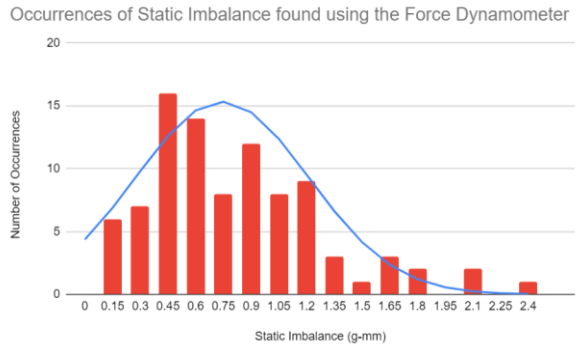

Figure 12: Histogram and Normal Distribution of the RW-0.06 Products Static Imbalance Data Set found using the Force Dynamometer

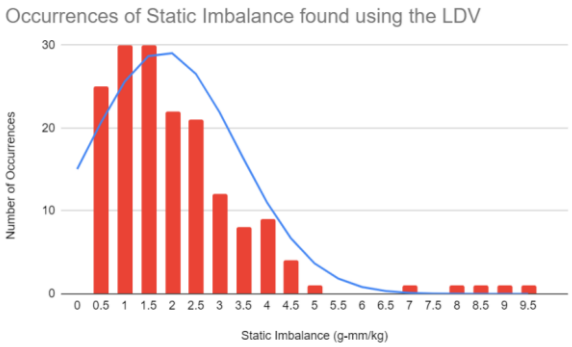

Figure 13: Histogram and Normal Distribution of the RW-0.06 Products Static Imbalance Data Set found using the Laser Doppler Vibrometer

The quality control limits found qualitatively were based on the micro-vibration profile values from rejected RW's. There are several qualitative measures that indicate if a RW micro-vibration profile is out of specification. An example would be to spin the RW's rotor manually to feel the imbalance and/or hear the noise generated from the RW itself. Another indicator are the waterfall plots and values for the noise profiles at different frequency ranges. The qualitative control limits were iterative throughout the growth of the dataset, which allowed for a better understanding of each RW's micro-vibration performance.

Utilizing an analytical approach over a qualitative approach can potentially lead to statistically categorizing a RW's micro-vibration performance as outside of the acceptable control limits, even if the RW's performance is acceptable by qualitative measures. However, it is evident from Tables 4 and 5 that the qualitative and analytical quality control limits are predominantly in agreement. This indicates that there is sufficient quality assurance in the control limits set qualitatively and that these limits can continue to be used for the production of the RW-0.06 product.

Table 4: Quality Control Limits for the RW-0.06 Products Data Set, from Measurements using the Force Dynamometer

Force Dynamometer Limits	Analytical	Qualitative
Static Imbalance (g-mm)	< 2.1	< 2.0
Total Fx Force 100 - 150 Hz at 600 rad/s (N rms)	< 0.0007	< 0.0004
Total Fx Force 120 - 700 Hz (N rms)	< 0.03	< 0.02
Total Fz Force 120 - 700 Hz (N rms)	< 0.02	< 0.01

Table 5: Quality Control Limits for the RW-0.06 Products Data Set, from Measurements using the Laser Doppler Vibrometer

Laser Doppler Vibrometer	Analytical	Qualitative
Static Imbalance (g-mm/kg)	< 6.5	< 7.0
Low Frequency 100-150 Hz (G rms)	< 0.001	< 0.001
Medium Frequency 150-2000 Hz (G rms)	< 0.18	< 0.20
High Frequency 2000-10000 Hz (G rms)	< 0.73	< 0.70

Correlation Analysis

It is important to note that a direct comparison between the force dynamometer and the LDV cannot be made due to the differences in the methods of measurement. In the case of the LDV, it is not clear what mass is being excited during the test, whether it be the entire mass of the RW or the rotating mass.

To determine the weight of the mass being excited during these tests, the full RW-0.06 data set from both test methods were plotted on the same graph. The static imbalance found using the force dynamometer is on the

y-axis and the static imbalance using the LDV is on the x-axis (seen in Figure 14).

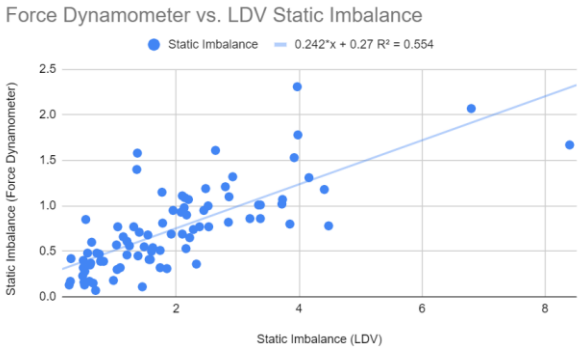

Figure 14: Correlation Graph of the Static Imbalances found in a Data Set (85 points), using the Force Dynamometer (y-axis) and Laser Doppler Vibrometer (x-axis)

From the correlation graph, the best-fit line equation is determined to be:

$$0.242x + 0.27 \quad (16)$$

The slope of the best-fit line is assumed to be equal to the weight of the mass excited in the tests, which would be 0.242kg. This result is reasonable as the approximate weight of the RW-0.06 wheel is around 0.235kg. The discrepancy could be due to added weight from the RW's harness when performing the test.

To convert the LDV static imbalance data from gram-mm/kg to gram-mm, the best fit line (Equation 16) was used; where x was the static imbalance found using the LDV. This calculation was performed for each RW's static imbalance in the LDV dataset, resulting in a new scaled LDV dataset. The error in static imbalance between the LDV and force dynamometer was then calculated for each RW. The standard deviation of the static imbalance error was ~0.31, and the 3-sigma value was ~0.93. The 3-sigma value was then subtracted from the force dynamometers static imbalance quality control limit. This calculation resulted in a new quality control limit for the scaled LDV static imbalance dataset, which was < 1.07.

This quality control limit indicates which RW units tested with the LDV, are likely to be rejected when tested with the force dynamometer. This limit, when applied to the scaled LDV dataset, results in 14 out of 85 RWs failing and being flagged for further testing using the force dynamometer. Of the 14 RW's flagged, 2 of the RW's were rejected after testing with the force dynamometer. This indicates that the new quality control limit for the scaled LDV static imbalance measurements can be used in the production environment to constrict the RW units that would require testing with the force dynamometer.

The coefficient of determination (R^2) is 0.554 and was used to determine the correlation coefficient (R) which is 0.74. This R value indicates a strong linear relationship between the force dynamometer and LDV measurements for the static imbalance measurements.

Case Study

The waterfall plots and frequency graphs from the force dynamometer and LDV, respectively, can be used to qualitatively inspect the data. The static imbalance and noise profile can be used to quantitatively assess the data using the pass/fail criteria determined by the quality control limits. The case study below shows the use of both methods to determine if a RW's micro-vibration profile is acceptable throughout its manufacturing. It is important to note that a RW can be rejected even if the static imbalance is acceptable, but the noise profiles are not, and vice versa. In Tables 5 and 6, the results of two RW-0.06 products from the Force Dynamometer and the LDV respectively, are shown.

Table 6: A comparison of Unit A and Unit B using the Pass/Fail Criteria for the Force Dynamometer

Force Dynamometer	**Unit A**	**Unit B**
Criteria	**Pass**	**Fail**
Static Imbalance (g-mm)	0.3 g-mm	0.9
Total Fx Force 100 - 150 Hz at 600 rad/s (N rms)	1.46e-04	4.01e-04
Total Fx Force 120 - 700 Hz (N rms)	4.95e-03	6.61e-02
Total Fz Force 120 - 700 Hz (N rms)	3.68e-03	1.97e-02
Mid-Frequency Force (NRMS)	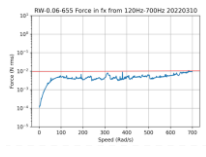	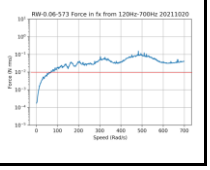

Waterfall Plot	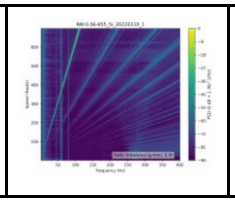	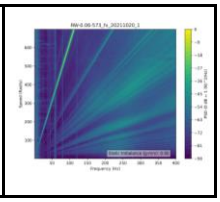

Table 7: A comparison of Unit A and Unit B using the Pass/Fail Criteria for the Laser Doppler Vibrometer

Laser Doppler Vibrometer	Unit A	Unit B
Criteria	**Pass**	**Fail**
Static Imbalance (g-mm/kg)	1.04	2.17
Low Frequency 100-150 Hz (G rms)	1.55e-04	1.31e-03
Medium Frequency 150-2000 Hz (G rms)	5.19e-02	3.05e-01
High Frequency 2000-10000 Hz (G rms)	3.68e-01	7.10e-01

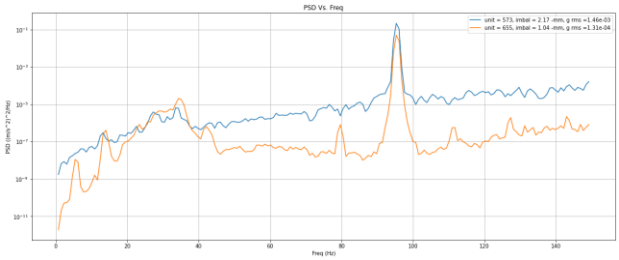

Figure 15: PSD vs. Frequency Graphs in the Low Frequency Range, for Unit A (orange) and Unit B (blue), found with the Laser Doppler Vibrometer.

From this comparison, Wheel A is acceptable for all parameters using both methods. For Wheel B, the static imbalance is the only acceptable parameter, and the other parameters fail based on the criteria for both test methods.

The wheel that failed did so in both test methods, due to the bearing noise profile across all relevant frequency ranges. This indicates that the quality control limits for both the static imbalance and noise profiles are equally important in determining if the RW micro-vibration profile is acceptable.

CONCLUSIONS AND FUTURE WORK

This paper presented a two-step process for characterizing and verifying a RWs micro-vibration performance using a Multicomponent Force Dynamometer and a Laser Doppler Vibrometer, respectively. Analysis of the data collected using the force dynamometer's time domain and the LDV's frequency domain data was presented. The imbalances for the time domain data were found using coherent integration to improve the SNR. A large set of data was collected using the RW-0.06 products manufactured by Sinclair Interplanetary, to perform the analyses presented in this paper.

Quality control limits were found both analytically and qualitatively for both methods based on the imbalance and noise profile values in the dataset. It was determined that the quality control limits found both statistically and qualitatively agree. This indicates that the qualitative limits currently used in the production environment are effective in determining the pass/fail criteria of a RW's micro-vibration performance. A correlation analysis between the two test methods was conducted to find the correction factor for scaling the LDV dataset, and to compute a new quality control limit for the scaled LDV dataset. This proved to be successful in constricting the number of RW's that would need to be tested using both test methods in a production environment. It was also found that there is a strong correlation of 0.74, between the data sets from both methods. The results of these analyses are promising in refining the two-step process to be more efficient in a production environment.

The proposed refined two-step process for verifying the RW micro-vibration profile can be implemented as follows:

1) Throughout the acceptance testing phase of the product, the RW is tested using the LDV to verify the micro-vibration profile.

2) At each step, the data is processed, and the static imbalance is scaled. The scaled data is then assessed using the new quality control limit for the scaled LDV data.

3) If the static imbalance is below the control limit, the micro-vibration profile is suitable and the RW can continue progressing in production. If the static imbalance is above the control limit, the micro-vibration profile is not suitable, and the unit has failed. A failed unit is unable to continue progressing in production.

4) If the unit has failed, the product should then be tested using the Multicomponent Force Dynamometer to try to determine the failure mode. The processed data from this test can be used to diagnose and correct for the product's failure mode.

Future research can consider scaling the LDV's noise profile and determine the scaled quality control limits for the LDV, using a similar method as provided in the correlation analysis section. This would strengthen the proposed refined two-step process, as there would be more metrics to consider for the scaled LDV's pass/fail criteria.

The methods provided here can be used by those in the small satellite community to verify and characterize a Reaction Wheel's micro-vibration profile. The effects of micro-vibrations on a spacecraft can be detrimental to a mission. As production of Reaction Wheel products are scaled up, it is vital to accurately verify the micro-vibration profile of these components in an efficient manner.

REFERENCES

1. Tkachev, S. et al. "Effect of Reaction Wheel Imbalances on Attitude and Stabilization Accuracy" Aerospace, Vol. 8, No. 9, 2 Sept. 2021

2. Shields, J. et al. "Characterization of CubeSat Reaction Wheel Assemblies" JoSS, Vol. 6, No. 1, pp. 565–580, 2017

3. Le, M. P. "Micro-Disturbances in Reaction Wheels." Technische Universiteit Eindhoven, 21 Mar. 2017

4. HBM. "Piezoelectric or Strain Gauge Based Force Transducers?" HBM, 2 June 2017

5. Zwolinski, B. "Practical Considerations of Multicomponent Force Measurements for Space Applications," Kistler, 2 Dec. 2021

6. Polytec. "The Basic Principles of Vibrometry". AZoSensors. 21 Nov. 2016